THE ASTROPHYSICAL JOURNAL, 249:109–117, 1981 October 1

ULTRAVIOLET INTERSTELLAR EXTINCTION TOWARD STARS IN THE ORION NEBULA AND TOWARD HD 147889

RALPH C. BOHLIN[1]
Laboratory for Astronomy and Solar Physics, Goddard Space Flight Center
AND
BLAIR D. SAVAGE[1]
Washburn Observatory, University of Wisconsin-Madison
Received 1981 February 9; accepted 1981 April 7

ABSTRACT

The *International Ultraviolet Explorer* (*IUE*) was used to obtain low resolution absolute ultraviolet energy distributions for the four Trapezium stars θ^1 Orionis A, B, C, and D, θ^2 Orionis A and B, HD 147889, and several unreddened standard stars. The observations for θ^1 Orionis B reveal a peculiar extended object. The measurements for the rest of the stars were used to derive UV extinction curves. The derived curves are very different from the average galactic curve. The curves for the Orion stars all exhibit smaller than normal middle and far-UV extinctions. Although a 2175 Å feature is present, its strength, when normalized to $E(B-V)$, is smaller than in the average galactic curve. In contrast, the curve for HD 147889 has a pronounced 2175 Å feature followed by smaller than normal extinction between $\lambda^{-1} = 5$ and 7 μm^{-1}. The curve for HD 147889 follows the *OAO 2* curves for σ Sco and ρ Oph down to $\lambda^{-1} \approx 6$ μm^{-1} and then abruptly turns upward. The pronounced differences in the character of interstellar UV extinction from region to region, and even within a region, can lead to large errors when an average galactic curve is used to correct for the presence of dust in observed UV energy distributions.

Subject headings: interstellar: matter — nebulae: Orion Nebula — spectrophotometry — stars: early-type — stars: individual — ultraviolet: spectra

I. INTRODUCTION

The correction of astronomical data for the effects of extinction produced by interstellar dust is a fundamental problem of observational astronomy. This problem is particularly severe in the UV because of the large absorption and scattering efficiencies of interstellar dust particles at short wavelengths and because of large apparent differences in the shape of the UV extinction curve. New insights may be obtained by studying the extinction properties of dust in disturbed galactic regions.

In this paper, measurements of UV interstellar extinction toward two interesting regions are presented. One region is the Orion Nebula and the other is toward the star HD 147889, a heavily reddened star in the ρ Oph reflection nebula. The UV extinction curves obtained are significantly different from the average galactic curve of Savage and Mathis (1979).

II. ULTRAVIOLET SPECTRAL ENERGY DISTRIBUTIONS

The data for this investigation were obtained with the *International Ultraviolet Exporer* (*IUE*) operating in the low resolution mode, which provides a resolution of ~ 7 Å from 1200 to 2000 Å with the short wavelength prime (SWP) camera and from 1900 to 3200 Å with the long wavelength redundant (LWR) camera. For details about the instrument and its performance see Boggess *et al.* (1978*a*, *b*) and Bohlin *et al.* (1980). The stars observed are listed in Table 1. In order of preference, the sources for the spectral classifications and ground based photometry are Lesh (1968, 1972), Blanco *et al.* (1970), and Hoffleit (1964). The listed values of the color excess $E(B-V)$ assume that the intrinsic colors are those as given by Johnson (1966). The SWP and LWR images obtained are also listed. In general, data were obtained with both the large (10″ × 20″) and small (3″) aperture is indicated in the table.

For some of the bright stars of this investigation the exposure times were short and the timing accuracy of the *IUE* must be carefully considered. The actual *IUE* exposure time is not as specified but is truncated to multiples of 0.4096 s (Bohlin *et al.* 1980). In addition, the true exposure times are shorter by 0.12 s, which is the difference between the high voltage power supply rise and fall times, as determined independently by Shiffer (1980) and in the course of this investigation. The only known remaining uncertainty in exposure times is 30 ms due to the commanding uncertainty of one cycle of the on-board computer. Thus, for the shortest exposure of 0.70 s used in this investigation, the 30 ms uncertainty causes a maximum error in the *IUE* response of $\pm 4\%$, comparable to the intrinsic 2 σ photometric stability of SWP temperature corrected spectra in the large aperture

[1] Guest Observer with the *International Ultraviolet Explorer* satellite which is sponsored and operated by the National Aeronautics and Space Administration, by the Science Research Council of The United Kingdom, and by the European Space Agency.

TABLE 1

STARS OBSERVED

HD	NAME	S.T.	V	$B-V$	$E(B-V)$	*IUE* IMAGES (aperture)[a] SWP	*IUE* IMAGES (aperture)[a] LWR	EXPOSURE TIMES[b] SWP	EXPOSURE TIMES[b] LWR	C[c]
3360[d]	ζ Cas	B2 IV	3.68	−0.20	0.04	4316(S, L), 5371(S)	1471(L), 1472(L), 3812(S, L)	0.96	0.24, 0.38, 0.77	−2.0
34816[d]	λ Lep	B0.5 IV	4.29	−0.25	0.03	1495(L), 1496(L)	...	0.29, 0.37	...	...
37020	θ^1 Ori A	B0.5 Vp	6.72	0.00	0.28	4282(S, L)	3783(S, L)	6.84	5.61	+1.2
37021	θ^1 Ori B	B3?	7.96	+0.24	0.44?	4283(S)[e]	3784(S, L), 3785(S)[d]	10.5	57.8	+1.4
37022	θ^1 Ori C	O6ep	5.13	0.00	0.32	1394(L), 4280(S, L)	1349(S), 1350(S, L), 1351(S, L)	0.70	1.52, 0.70	−0.4
37023	θ^1 Ori D	B0.5 Vp	6.70	+0.08	0.36	1403(L), 4281(S, L)	1352(L), 3782(S, L)	3.57	5.61	0.0
37041	θ^2 Ori A	O9.5 Vep	5.08	−0.11	0.19	1389(S, L)	1344(S, L), 3781(S, L)	0.70	0.70	+1.4
37042	θ^2 Ori B	B0.5 V	6.38	−0.09	0.19	4278(S, L)	1368(S, L), 3780(S, L)	2.75	2.75	+1.4
38666[d]	μ Col	O9.5 IV	5.16	−0.29	0.01	1210(S, L), 1211(S, L)	1197(S, L), 1198(S, L)	0.82, 1.34	0.87, 1.67	−1.2
120315[d]	η UMa	B3 V	1.84	−0.18	0.02	2341(L), 4110(L)	2127(S, L), 3079(S), 3640(L)	0.36, 0.27	0.25, 0.23	−3.0
147889	...	B2 V	7.86	+0.85	1.09	2793(L), 4338(S, L)	2482(S), 2483(S), 3831(S, L)	420	900	0.0

[a] S denotes small, 3″ aperture. L denotes large, 10″ × 20″ aperture.

[b] Exposure times for the large aperture data in seconds. The small aperture SWP 4283 for θ^1 Ori B was normalized to the LWR data, so that the effective exposure time listed can be used for the absolute calibration.

[c] Normalization constants for Figs. 1 and 2.

[d] Standard comparison star.

[e] Large aperture spectra on SWP 4283 and LWR 3785 were overexposed, except at the wavelength extremes. Spectra obtained in eclipse are on SWP 4341 through SWP 4343.

(Bohlin *et al.* 1980). In summary, the worst case photometric error due to the 2 σ uncertainty of 6% for LWR and the 30 ms uncertainty for a 0.70 s exposure should be less than 10%.

The *IUE* spectra used in this study (see Table 1) with image numbers below 2000 for both cameras were reduced during the first weeks of operation with a preliminary Intensity Transfer Function (ITF) and delivered to the official NASA and ESA data centers. This preliminary ITF has indeterminate linearity properties and a poorly known photometric calibration, which render these data inappropriate for studies of absolute (or relative) flux distributions. Consequently, all the early Orion images were reprocessed using the Guest Observer funds for this program. The reprocessed spectra were not delivered to the data centers, because no policy for this unique situation exists. Subsequent to this reprocessing and the standard processing of the remainder of the data, an error in the ITF for the SWP camera was discovered. All Guest Investigator SWP data were then corrected using the approved correction algorithm for low dispersion (Cassatella *et al.* 1980). The standard star spectra were reprocessed with the corrected SWP ITF. The final *IUE* absolute fluxes use the temperature correction to the sensitivity of $-0.8\%\ ^\circ C^{-1}$ (Bohlin *et al.* 1980) and the updated absolute calibration of Bohlin and Holm (1980).

The *IUE* data listed in Table 1 were combined to produce the absolute energy distributions shown in Figures 1 and 2 with wavelength bins 5 Å wide. Table 2 lists a 25 Å average of the fluxes plotted in Figures 1 and 2. The absolute flux distributions are a mean of all data for each star, weighted by the observed signal strength. The mean of all large aperture data defines the overall absolute level. The small aperture data are used to refine the shape by normalizing to the mean of the large aperture in the range 1600–1725 Å for SWP and 1950–2150 Å for LWR. All saturated data and spectral data near reseau marks are given zero weight in the final mean. In the case of θ^1 Ori A, another star (θ^1 Ori C) appears in the large aperture; and a special extraction was used to obtain the pure spectrum of θ^1 Ori A from the line-by-line file of *IUE* data.

The effects of interstellar extinction are apparent in Figures 1 and 2. The flux curves for the lightly reddened comparison stars (ζ Cas, μ Col, and η UMa) have no depression near the interstellar 2200 Å feature. In contrast, for the Orion stars the 2200 Å interstellar feature is readily apparent in the flux curves for the Trapezium stars (θ^1 Ori A, B, C, D) and less apparent in the curves for the two stars outside the Trapezium (θ^2 Ori A and B). The heavily reddened star HD 147889 (B2 V) has an energy distribution that is dominated by the effects of UV extinction. The depression in flux near 2200 Å and for $\lambda \lesssim 1500$ Å is striking.

The strengths of the stellar Si IV λ1400 and C IV λ1550 lines seen in the flux curves of Figures 1 and 2 appear generally consistent with the classifications listed in Table 1 and the line strength versus spectral type calibration of Panek and Savage (1976). The strong feature near 1540 Å in the curve for HD 147889 is not real. One of the images (SWP 2793) used to produce this spectrum had a transmission dropout at 1540 Å.

The *IUE* data on the eclipsing binary θ^1 Ori B are enigmatic. The approximate spectral classification of B3

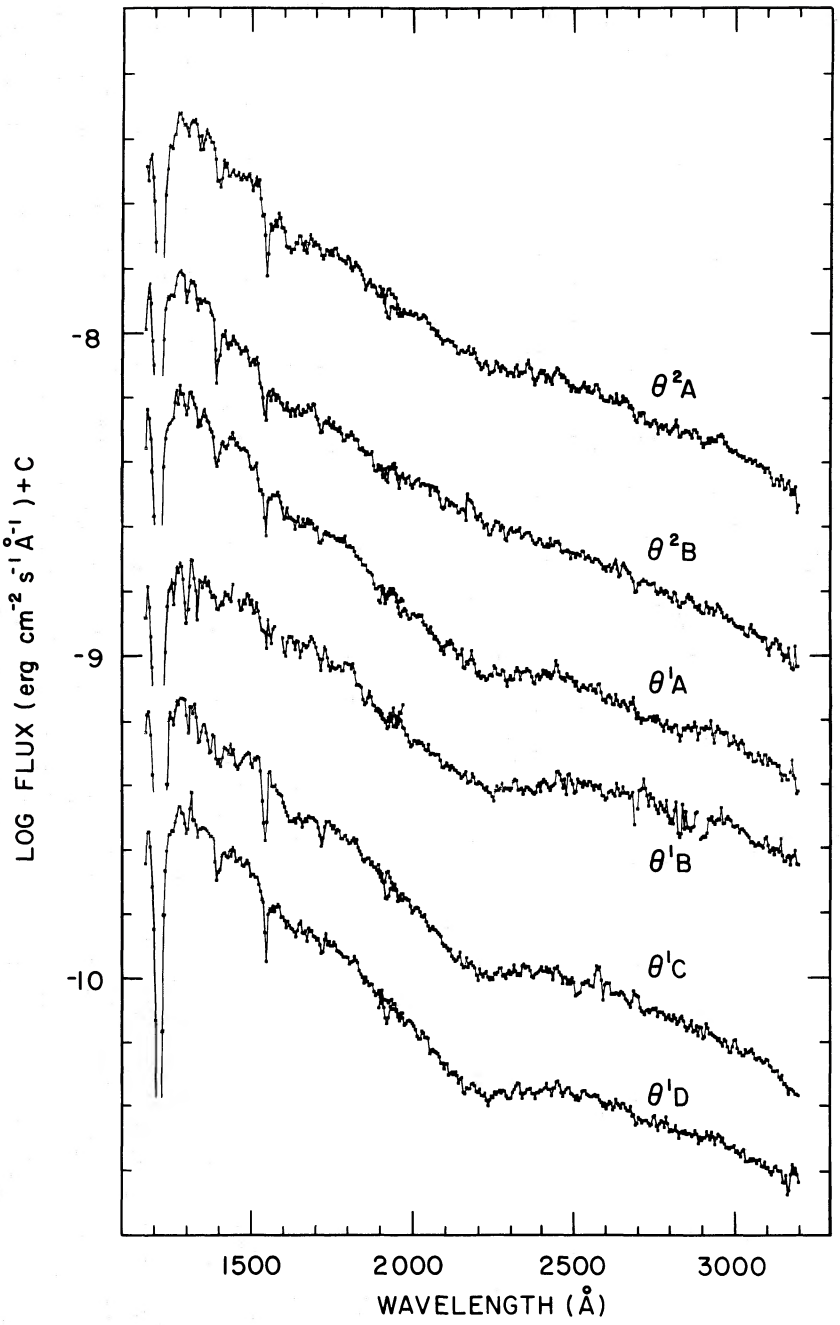

FIG. 1.—Ultraviolet flux distributions for six Orion stars. Log F_λ (ergs cm^{-2} s^{-1} Å^{-1}) + C is plotted versus λ in Å. The value of the constant, C, for each star is given in Table 1. The effects of extinction are readily apparent in the broadband extinction depression near 2175 Å.

is verified by the strengths of the lines of Si III (1300 Å) and C IV (1550 Å), as can be seen by comparing the spectrum taken out of eclipse in Figure 1 with the spectrum of η UMa (B3 V) in Figure 2. Although the spectra are not illustrated here, the lines in additional *IUE* data obtained during eclipse are also of similar strengths. The most puzzling observation is that all three large-aperture spectra taken out of eclipse are spatially extended, with a FWHM of $6''.8 \pm 0.3$, compared to the normal point spread function with a FWHM = $4''.8 \pm 0.3$ for the nominal focus condition at the times of observation. An angular size of $2''$ translates to 1000 AU at the distance of 500 pc to Orion. Large aperture observations centered on θ^1 Ori B revealed the presence of a second source located $\sim 9''$ southeast of θ^1 Ori B. However, no star is located at this position on the

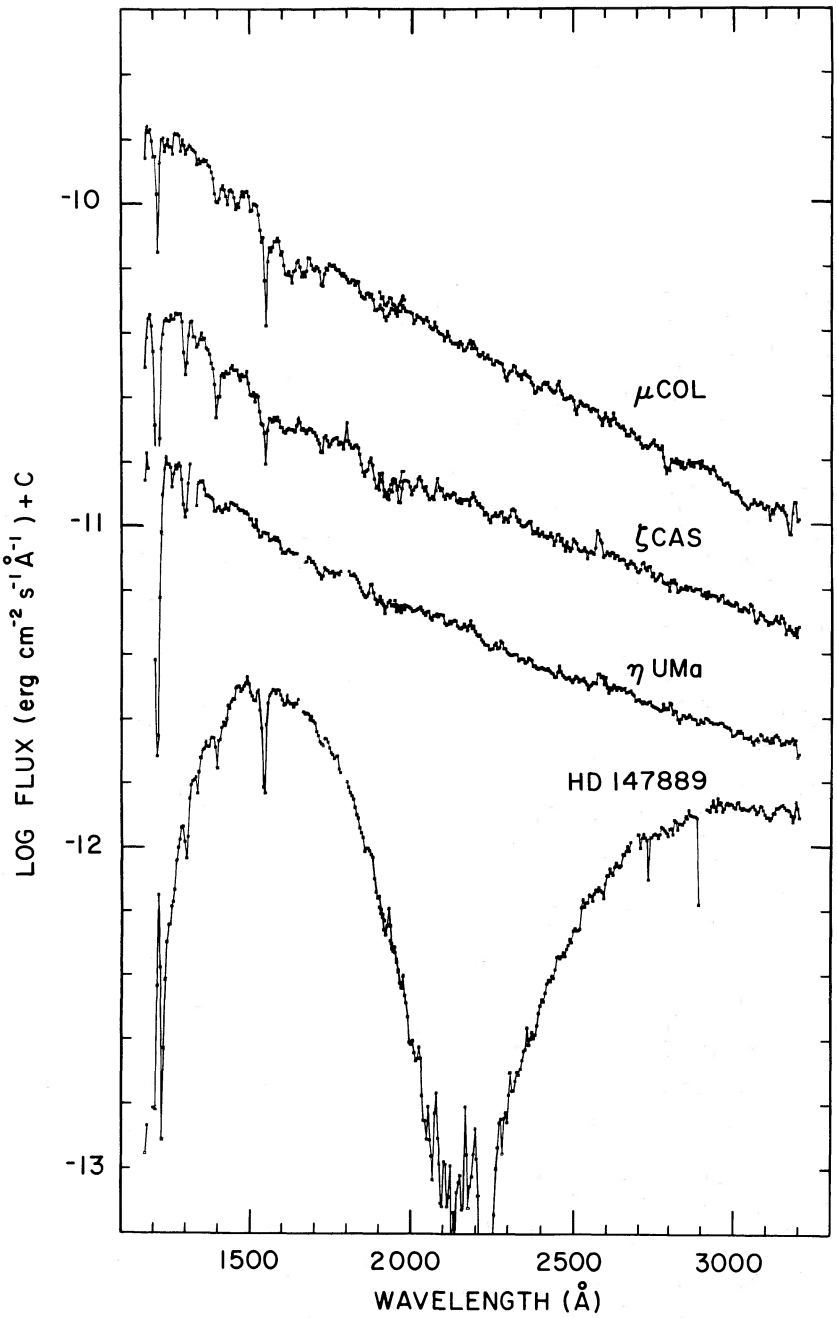

FIG. 2.—Ultraviolet flux distributions for three lightly reddened comparison stars and the heavily reddened star HD 147889. Log F_λ (ergs cm^{-2} s^{-1} Å^{-1}) + C is plotted versus λ in Å. The value of the constant C for each star is given in Table 1. The feature near 1550 Å in HD 147889 is not real but due to a transmission dropout in one of the images (SWP 2973) used to construct the mean spectrum. The effects of interstellar extinction dominate the energy distribution for HD 147889.

photographs of Feibelman and Gull (1978). This suggests that we may have detected a transient phenomenon in the UV on 1979 February 17. The absolute UV energy distribution of θ^1 Ori B out of eclipse was ~ 1 mag brighter than expected for the visual magnitude of 7.96, if we require consistency with the typical extinction curve in Orion and the 2200 Å extinction feature observed in the θ^1 Ori B spectrum. The absolute flux from θ^1 Ori B during eclipse, as measured on 1979 February 22–23, is consistent with $V = 7.96$ and the depth of the eclipse of 0.6 mag in the visual (Hall and Garrison 1969); i.e., there is about 1.6 mag difference between the *IUE* fluxes in and out of eclipse. Wilson (1972), who uses the name BM Ori for θ^1 Ori B, has suggested that the binary may contain a black hole. More study of this system is needed, and an additional publication on this subject is intended.

TABLE 2

ABSOLUTE ENERGY DISTRIBUTIONS (in ergs cm^{-2} s^{-1} $Å^{-1}$)

λ (Å)	ζ CAS	λ LEP	θ^1ORI A	θ^1ORI B	θ^1ORI C	θ^1ORI D	θ^2ORI A	θ^2ORI B	μ COL	η UMA	HD147889
SWP											
1200	3.17E-09		1.66E-10	2.30E-11	7.50E-10	1.33E-10	9.67E-10	2.99E-10	2.28E-09		
1225	2.91E-09	4.16E-09	1.43E-10	1.57E-11	3.66E-10	9.24E-11	4.05E-10	2.37E-10	2.12E-09	9.08E-09	3.74E-13
1250	4.48E-09	4.96E-09	3.32E-10	6.18E-11	1.51E-09	2.76E-10	1.48E-09	5.17E-10	2.44E-09	1.52E-08	5.95E-13
1275	4.54E-09	5.06E-09	4.15E-10	7.33E-11	1.81E-09	3.31E-10	1.81E-09	6.01E-10	2.59E-09	1.52E-08	9.70E-13
1300	3.59E-09	4.67E-09	3.84E-10	5.94E-11	1.75E-09	3.14E-10	1.68E-09	5.51E-10	2.38E-09	1.22E-08	1.13E-12
1325	3.98E-09	4.62E-09	3.76E-10	6.82E-11	1.64E-09	3.34E-10	1.74E-09	5.29E-10	2.28E-09		1.59E-12
1350	3.82E-09	4.36E-09	3.44E-10	6.75E-11	1.47E-09	2.92E-10	1.57E-09	5.02E-10	2.15E-09	1.35E-08	1.96E-12
1375	3.37E-09	4.17E-09	3.27E-10	6.35E-11	1.37E-09	2.78E-10	1.57E-09	4.70E-10	2.04E-09	1.23E-08	2.14E-12
1400	2.59E-09	3.13E-09	2.61E-10	5.74E-11	1.20E-09	2.20E-10	1.21E-09	3.39E-10	1.65E-09	1.12E-08	2.10E-12
1425	2.98E-09	3.42E-09	2.86E-10	6.05E-11	1.29E-09	2.42E-10	1.29E-09	3.79E-10	1.68E-09	1.13E-08	2.57E-12
1450	3.07E-09	3.48E-09	2.96E-10		1.17E-09	2.38E-10	1.25E-09	3.74E-10	1.59E-09	1.17E-08	2.98E-12
1475	2.92E-09	3.35E-09	2.75E-10	5.73E-11	1.20E-09	2.28E-10	1.20E-09	3.53E-10	1.63E-09	1.11E-08	3.14E-12
1500	2.70E-09	3.03E-09	2.49E-10	5.87E-11	1.20E-09	2.17E-10	1.17E-09	3.31E-10	1.60E-09	1.05E-08	3.09E-12
1525	2.37E-09	2.71E-09	2.24E-10	5.33E-11	1.12E-09	1.93E-10	1.09E-09	3.03E-10	1.42E-09	9.69E-09	2.80E-12
1550	1.94E-09	2.08E-09	1.79E-10	4.66E-11	8.76E-10	1.49E-10	7.75E-10	2.41E-10	1.00E-09	9.39E-09	2.24E-12
1575	2.16E-09	2.30E-09	1.99E-10		9.57E-10	1.64E-10	8.68E-10	2.58E-10	1.19E-09	9.09E-09	3.06E-12
1600	2.04E-09	2.16E-09	1.80E-10		8.89E-10	1.54E-10	8.25E-10	2.38E-10	1.09E-09	8.41E-09	2.90E-12
1625	2.00E-09	1.99E-09	1.69E-10	4.47E-11	7.76E-10	1.43E-10	7.22E-10	2.31E-10	9.48E-10	8.29E-09	2.82E-12
1650	2.05E-09		1.61E-10	4.19E-11	7.72E-10	1.42E-10	7.70E-10	2.29E-10	1.00E-09		
1675	2.00E-09		1.62E-10	4.29E-11	7.78E-10	1.37E-10	7.47E-10	2.31E-10	1.02E-09		2.59E-12
1700	1.93E-09	1.98E-09	1.58E-10	4.31E-11	7.68E-10	1.34E-10	7.52E-10	2.29E-10	9.99E-10	7.50E-09	2.40E-12
1725	1.80E-09	1.87E-09	1.44E-10	3.92E-11	6.97E-10	1.25E-10	6.97E-10	2.06E-10	9.38E-10	7.10E-09	2.13E-12
1750	1.82E-09	1.93E-09	1.48E-10	3.71E-11	7.49E-10	1.27E-10	7.08E-10	2.09E-10	1.01E-09	7.11E-09	1.99E-12
1775	1.82E-09		1.44E-10	3.62E-11	6.84E-10	1.21E-10	6.70E-10	1.91E-10	9.51E-10		
1800	1.94E-09		1.44E-10	3.70E-11	6.73E-10	1.15E-10	6.60E-10	1.92E-10	9.36E-10		
1825	1.76E-09	1.80E-09	1.31E-10	3.45E-11	6.58E-10	1.13E-10	6.40E-10	1.89E-10	9.02E-10	6.88E-09	1.33E-12
1850	1.52E-09	1.65E-09	1.22E-10	2.97E-11	6.00E-10	1.01E-10	5.82E-10	1.72E-10	8.11E-10	6.13E-09	1.05E-12
1875	1.53E-09	1.61E-09	1.12E-10	2.90E-11	5.72E-10	9.48E-11	5.63E-10	1.66E-10	7.85E-10	6.27E-09	9.24E-13
1900	1.37E-09	1.44E-09	1.02E-10	2.62E-11	5.25E-10	8.81E-11	5.19E-10	1.51E-10	7.47E-10	5.79E-09	6.73E-13
1925	1.24E-09		9.73E-11	2.44E-11	4.52E-10	7.51E-11	4.54E-10	1.41E-10	7.11E-10		
LWR											
1925	1.29E-09		9.65E-11	2.52E-11	5.13E-10	8.49E-11	5.25E-10	1.50E-10	7.84E-10	5.61E-09	5.71E-13
1950	1.32E-09		9.76E-11	2.46E-11	4.57E-10	8.19E-11	4.92E-10	1.55E-10	7.32E-10	5.40E-09	4.45E-13
1975	1.35E-09		8.32E-11	2.42E-11	4.43E-10	7.28E-11	4.50E-10	1.42E-10	7.31E-10	5.56E-09	3.71E-13
2000	1.32E-09		8.32E-11	2.14E-11	4.18E-10	7.26E-11	4.57E-10	1.37E-10	7.06E-10	5.45E-09	2.53E-13
2025	1.37E-09		8.33E-11	2.13E-11	4.04E-10	6.64E-11	4.47E-10	1.38E-10	6.94E-10	5.45E-09	2.12E-13
2050	1.22E-09		7.63E-11	2.03E-11	3.73E-10	6.33E-11	4.29E-10	1.34E-10	6.78E-10	5.31E-09	1.24E-13
2075	1.25E-09		7.24E-11	1.95E-11	3.50E-10	5.75E-11	3.98E-10	1.28E-10	6.32E-10	5.17E-09	1.23E-13
2100	1.25E-09		6.60E-11	1.81E-11	3.25E-10	5.42E-11	3.76E-10	1.17E-10	6.14E-10	5.04E-09	9.39E-14
2125	1.24E-09		6.81E-11	1.77E-11	3.00E-10	5.10E-11	3.71E-10	1.18E-10	5.88E-10	5.00E-09	7.81E-14
2150	1.19E-09		6.52E-11	1.69E-11	2.82E-10	4.86E-11	3.48E-10	1.15E-10	5.72E-10	4.84E-09	6.49E-14
2175	1.19E-09		5.88E-11	1.64E-11	2.77E-10	4.46E-11	3.52E-10	1.19E-10	5.70E-10	4.83E-09	1.00E-13
2200	1.20E-09		5.88E-11	1.62E-11	2.65E-10	4.56E-11	3.35E-10	1.10E-10	5.54E-10	4.62E-09	1.06E-13
2225	1.10E-09		5.39E-11	1.55E-11	2.59E-10	4.32E-11	3.16E-10	1.03E-10	5.31E-10	4.27E-09	-2.29E-15
2250	1.06E-09		5.48E-11	1.46E-11	2.51E-10	4.22E-11	3.05E-10	9.78E-11	5.09E-10	4.16E-09	-9.63E-15
2275	1.07E-09		5.55E-11	1.53E-11	2.61E-10	4.41E-11	3.12E-10	1.00E-10	4.99E-10	4.20E-09	1.22E-13
2300	1.09E-09		5.32E-11	1.52E-11	2.57E-10	4.28E-11	3.00E-10	9.43E-11	4.64E-10	3.98E-09	1.60E-13
2325	1.10E-09		5.50E-11	1.57E-11	2.62E-10	4.57E-11	3.03E-10	9.68E-11	4.76E-10	3.89E-09	1.86E-13
2350	1.00E-09		5.54E-11	1.51E-11	2.69E-10	4.36E-11	3.10E-10	9.39E-11	4.65E-10	3.79E-09	2.32E-13
2375	9.24E-10		5.38E-11	1.49E-11	2.59E-10	4.44E-11	2.83E-10	9.15E-11		3.78E-09	2.54E-13
2400	9.44E-10		5.44E-11	1.57E-11	2.75E-10	4.51E-11	3.00E-10	8.95E-11	4.27E-10	3.57E-09	3.12E-13
2425	9.25E-10		5.47E-11	1.55E-11	2.63E-10	4.49E-11	2.85E-10	8.77E-11	4.25E-10	3.50E-09	3.76E-13
2450	9.05E-10		5.69E-11	1.68E-11	2.62E-10	4.63E-11	2.97E-10	8.85E-11	4.22E-10	3.46E-09	4.30E-13
2475	8.69E-10		5.35E-11	1.59E-11	2.44E-10	4.41E-11	2.86E-10	8.34E-11	3.94E-10	3.35E-09	4.68E-13
2500	8.70E-10		5.27E-11	1.57E-11	2.40E-10	4.34E-11	2.67E-10	8.15E-11	3.77E-10	3.30E-09	5.31E-13
2525	8.38E-10		5.01E-11	1.59E-11	2.32E-10	4.31E-11	2.70E-10	8.24E-11	3.75E-10	3.27E-09	6.34E-13
2550	8.18E-10		4.95E-11	1.58E-11	2.41E-10	4.32E-11	2.65E-10	7.94E-11	3.65E-10	3.16E-09	6.81E-13
2575	9.12E-10		4.97E-11	1.54E-11	2.63E-10	4.29E-11	2.69E-10	7.73E-11	3.53E-10	3.38E-09	7.27E-13
2600	8.80E-10		4.69E-11	1.44E-11	2.43E-10	4.07E-11	2.47E-10	7.58E-11	3.40E-10	3.26E-09	7.57E-13
2625	8.08E-10		4.59E-11	1.50E-11	2.38E-10	4.04E-11	2.49E-10	7.54E-11	3.35E-10	3.10E-09	8.47E-13
2650	7.86E-10		4.47E-11	1.49E-11	2.23E-10	4.02E-11	2.44E-10	7.31E-11	3.19E-10	3.09E-09	8.95E-13
2675	7.57E-10		4.40E-11	1.46E-11	2.05E-10	3.78E-11	2.33E-10	6.80E-11	3.03E-10	2.95E-09	
2700	7.41E-10		4.25E-11		2.16E-10	3.60E-11	2.14E-10	6.37E-11	2.92E-10	2.84E-09	
2725	7.49E-10		3.95E-11	1.51E-11	1.96E-10	3.57E-11	2.16E-10	6.75E-11	2.77E-10	2.79E-09	1.06E-12
2750	7.20E-10		3.97E-11	1.42E-11	1.99E-10	3.57E-11	2.09E-10	6.56E-11	2.81E-10	2.73E-09	1.08E-12
2775	6.81E-10		3.87E-11	1.33E-11	1.95E-10	3.51E-11	2.02E-10	6.26E-11	2.60E-10	2.77E-09	1.11E-12
2800	6.54E-10		3.78E-11	1.25E-11	1.89E-10	3.48E-11	1.99E-10	6.08E-11	2.32E-10	2.72E-09	1.11E-12
2825	6.44E-10		3.71E-11	1.35E-11	1.86E-10	3.32E-11	2.00E-10	5.90E-11	2.44E-10	2.54E-09	1.18E-12
2850	6.37E-10		3.73E-11	1.34E-11	1.79E-10	3.30E-11	1.97E-10	5.91E-11	2.42E-10	2.55E-09	1.22E-12
2875	6.28E-10		3.77E-11	1.27E-11	1.76E-10	3.27E-11	1.95E-10	5.86E-11	2.45E-10	2.46E-09	1.18E-12
2900	6.18E-10		3.64E-11		1.68E-10	3.15E-11	1.83E-10	5.47E-11	2.45E-10	2.45E-09	
2925	5.97E-10		3.75E-11	1.10E-11	1.67E-10	3.25E-11	1.79E-10	5.59E-11	2.44E-10	2.45E-09	1.28E-12
2950	5.96E-10		3.62E-11	1.31E-11	1.61E-10	3.16E-11	1.84E-10	5.53E-11	2.23E-10	2.42E-09	1.35E-12
2975	5.81E-10		3.55E-11	1.21E-11	1.54E-10	3.02E-11	1.78E-10	5.23E-11	2.11E-10	2.37E-09	1.33E-12
3000	5.66E-10		3.39E-11	1.17E-11	1.49E-10	2.95E-11	1.71E-10	5.01E-11	2.00E-10	2.25E-09	1.34E-12
3025	5.55E-10		3.29E-11	1.12E-11	1.45E-10	2.83E-11	1.64E-10	4.79E-11	1.87E-10	2.23E-09	1.32E-12
3050	5.58E-10		3.07E-11	1.06E-11	1.47E-10	2.72E-11	1.60E-10	4.72E-11	1.83E-10	2.15E-09	1.32E-12
3075	5.15E-10		3.01E-11	1.02E-11	1.40E-10	2.69E-11	1.56E-10	4.60E-11	1.85E-10	2.18E-09	1.31E-12
3100	4.71E-10		2.99E-11	1.03E-11	1.36E-10	2.63E-11	1.50E-10	4.21E-11		2.08E-09	1.30E-12
3125	4.64E-10		2.90E-11	9.82E-12	1.27E-10	2.60E-11	1.38E-10	4.34E-11	1.67E-10	2.03E-09	1.29E-12
3150	4.98E-10		2.69E-11	9.59E-12	1.20E-10	2.43E-11	1.36E-10	4.06E-11	1.76E-10	2.11E-09	1.34E-12
3175	4.70E-10		2.71E-11	9.29E-12	1.12E-10	2.38E-11	1.31E-10	3.82E-11	1.63E-10	2.13E-09	1.26E-12
3200	4.83E-10		2.46E-11	8.99E-12	1.09E-10	2.39E-11	1.23E-10	3.92E-11	1.80E-10	2.07E-09	1.31E-12

III. EXTINCTION CURVES

For previous UV extinction measurements of stars in the Orion Nebula, contamination of the measurements by nebular light was potentially a serious problem (Bless and Savage 1972). Since no significant signal can be seen within the large entrance aperture on either side of the stellar spectra of the Orion stars, nebular scattering does not contaminate the fluxes derived from *IUE* data. For θ^1 Ori A, θ^1 Ori C, θ^1 Ori D, θ^2 Ori A, θ^2 Ori B, and HD 147889 the *IUE* large aperture spectra all have widths that resemble those produced by point stellar sources. For the Orion stars, this result is consistent with the long exposure times ($\sim$ 10 m) required to directly detect the nebular UV light. Unfortunately, the possibility of nebular contamination cannot be completely eliminated, since scattering that occurs within the 5″ spatial resolution of the *IUE* system would be interpreted as direct stellar radiation.

The normalized UV extinction curves shown in Figures 3 and 4 are derived from the energy distribution curves in Figures 1 and 2. In obtaining these curves the "pair method" is employed. The star pairs and corresponding values of ΔV and $\Delta(B-V)$ are listed in Table 3. In this method the normalized extinction is calculated from

$$\frac{E(\lambda-V)}{E(B-V)} = \left(2.5 \log \left[\frac{F_\lambda(C)}{F_\lambda(*)}\right] - \Delta V\right) \Big/ \Delta(B-V) ,$$

where $F_\lambda(C)$ and $F_\lambda(*)$ refer to the fluxes for the comparison star and reddened star, respectively, and the Δ's refer to differences between the star pairs. The pair method gives the correct result provided the reddened star and unreddened (or very lightly reddened) comparison star have identical intrinsic UV energy distributions. In practice, a perfect match is difficult to achieve, and mismatch errors may appear, even if the reddened and comparison stars are classified with identical spectral types. The size of possible mismatch errors will depend on the type of star under consideration. Meyer and Savage (1981) give a

TABLE 3

STAR PAIRS

Reddened Star	Comparison Star	ΔV	$\Delta(B-V)$
Cases Illustrated in Figures 3 and 4			
θ^1 Ori A	λ Lep	+2.43	0.25
θ^1 Ori C	μ Col	−0.03	0.29
θ^1 Ori D	λ Lep	+2.41	0.33
θ^2 Ori A	μ Col	−0.08	0.18
θ^2 Ori B	λ Lep	+2.09	0.16
HD 147889	ζ Cas	+4.18	1.05
Other Cases Computed			
θ^1 Ori B	η UMa	+6.12	0.42
θ^1 Ori C	θ^2 Ori A	+0.05	0.11
θ^1 Ori D	θ^2 Ori B	+0.32	0.17
θ^1 Ori D	θ^1 Ori A	−0.02	0.08

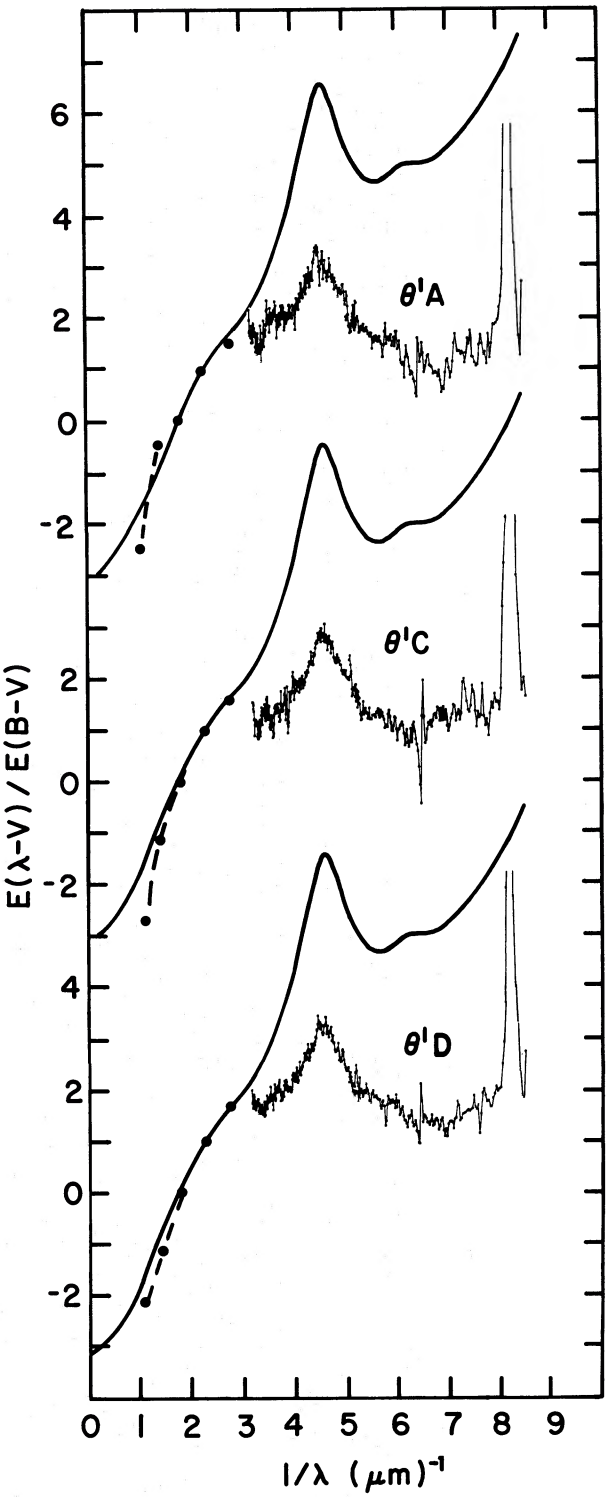

FIG. 3.—Normalized extinction, $E(\lambda - V)/E(B-V)$, versus $1/\lambda$ in μm^{-1}. The solid curve is the average extinction curve from Savage and Mathis (1979). The heavy filled circles are the ground based measurements of Lee (1968). The detailed *IUE* curves are indicated with the corresponding star name. Stellar and interstellar atomic lines introduce structure at $\lambda^{-1} = 6.45$ (C IV) and $\lambda^{-1} = 8.2$ (H I Lyα).

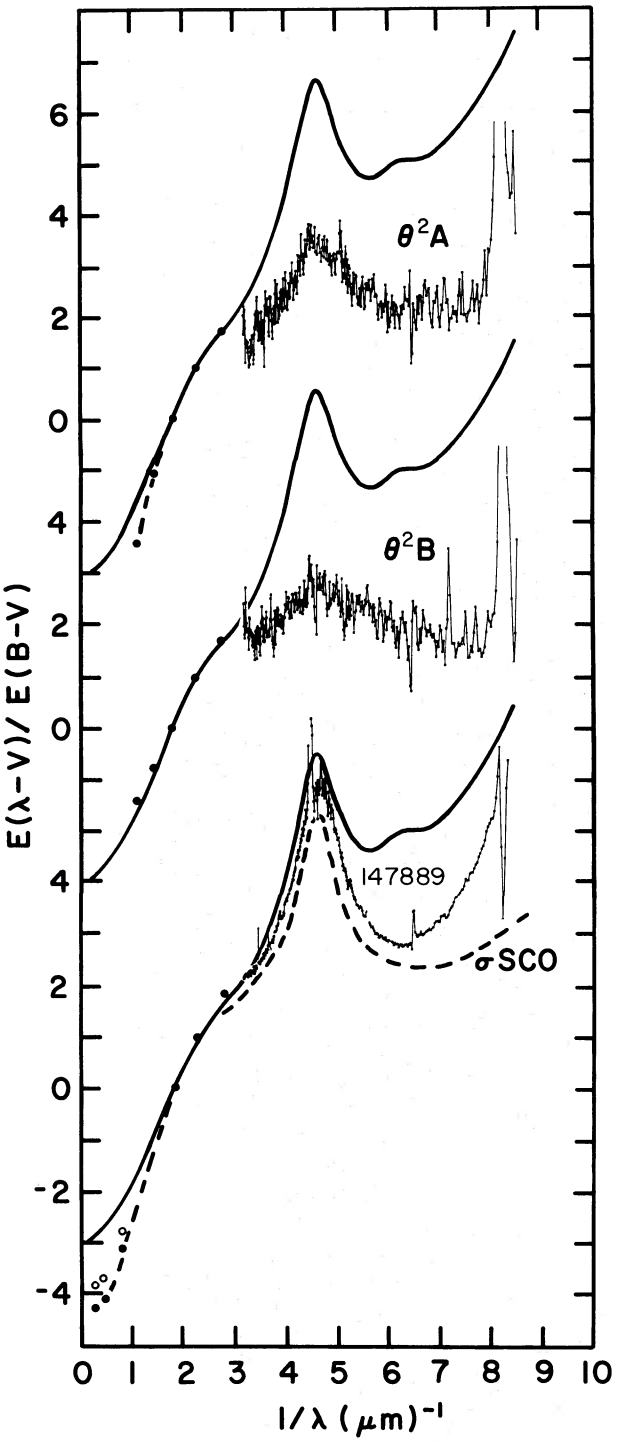

FIG. 4.—Normalized extinction, $E(\lambda - V)/E(B-V)$, is plotted versus $1/\lambda$ in μm^{-1}. The solid curve is the average extinction curve from Savage and Mathis (1978). The heavy filled circles are measurements from Lee (1968) for the Orion stars and from van Breda, Glass, and Whittet (1974) for HD 147889. The open circles illustrate additional infrared measurements from McMillan (1978) for HD 147889. The detailed *IUE* extinction curves are indicated with the corresponding star name. Stellar and interstellar atomic lines introduce structure at $\lambda^{-1} = 6.45$ (C IV) and $\lambda^{-1} = 8.2$ (H I Lyα). In the plot for HD 147889, the anomalous curve for σ Sco from Bless and Savage (1972) is also illustrated.

detailed discussion of errors associated with the derivation of extinction parameters and show that mismatch errors for stars B3 or hotter are typically ~ 0.15 mag for $\lambda > 2500$ Å and ~ 0.20 mag for $\lambda < 2500$ Å. In a *normalized* extinction plot, the mismatch error will therefore be $\sim 0.15/E(B-V)$ or $\sim 0.20/E(B-V)$, depending on the wavelength range. Additional errors include the uncertainty in $E(B-V)$ and the *IUE* photometric uncertainties. The $E(B-V)$ values probably have errors of ~ 0.03 while the *IUE* photometric uncertainties are less than 0.1 mag, as discussed above.

In the case of λ Lep, where *IUE* data are available from only the SWP camera, the *OAO 2* spectrum is used after converting the absolute fluxes to the *IUE* scale (Bohlin *et al.* 1980). The errors in this procedure are comparable to using *IUE* data for the comparison star, since the reproducibility for *OAO 2* is $2\sigma \sim 6\%$ (Strongylis and Bohlin 1979). The *IUE* data below 2000 Å for λ Lep agree with the *OAO 2* fluxes in that region.

a) The Orion Extinction

Baade and Minkowski (1937) first pointed out that the visual colors of the stars in the Trapezium of Orion are anomalous, and a number of other investigators have reached similar conclusions (Stebbins and Whitford 1945; Johnson 1968, 1977; Lee 1968; Anderson 1970). In Figures 3 and 4 the visual and infrared extinction data for the Orion stars were taken from Lee (1968). In the far-infrared, reliable extinction measurements of Orion stars are difficult to obtain because of potential contamination by heated nebular and/or circumstellar dust (Ney, Strecker, and Gehrz 1973). Consequently, the data for $\lambda^{-1} < 1.0\ \mu m^{-1}$ are not plotted in Figures 3 and 4.

The UV measurements of all five of the Orion stars have roughly similar extinction curves. The extinction throughout the UV, expressed as $E(\lambda - V)/E(B-V)$, is smaller than normal. The *IUE* Orion extinction curves, which should not be affected by contamination by nebular dust scattering and gaseous emission, are similar to the less reliable *OAO 2* measurement of Bless and Savage (1972), which referred to the combined radiation from θ^1 Ori A, B, C, and D and θ^2 Ori A and B.

The UV extinction curve for θ^1 Ori C lies somewhat lower than for the other stars. About 0.3 of this level shift may be associated with the total photometric uncertainty of 0.1 mag for the 0.70 s exposure times in the large aperture. The curves for θ^2 Ori A and B might have a slightly weaker 2200 Å feature than for θ^1 Ori A, C, and D. However, the normalized measurements for θ^2 Ori A and B are more uncertain, since $E(B-V)$ for these two stars is smaller (see Table 2).

Patriarchi and Perinotto (1980) have also presented Orion extinction curves using some of the *IUE* data presented here. Their normalized curves lie approximately 0.8 higher than those shown in Figures 3 and 4. Patriarchi and Perinotto did not allow for the electronics rise and fall time difference when deriving absolute fluxes and, in addition, used data processed with the preliminary ITF that was in effect before 1978 May. We consider the curves shown in Figures 3 and 4 more trustworthy.

TABLE 4

AVERAGE ORION EXTINCTION CURVE

λ (Å)	λ^{-1} (μm^{-1})	$E(\lambda-V)/E(B-V)$
3000	3.33	1.51
2740	3.65	1.81
2500	4.00	2.15
2400	4.17	2.39
2300	4.35	2.74
2190	4.57	3.09
2100	4.76	2.84
2000	5.00	2.43
1900	5.26	2.05
1800	5.56	1.83
1700	5.88	1.64
1600	6.25	1.50
1490	6.71	1.45
1390	7.18	1.52
1250	8.00	1.88

An average Orion extinction curve is listed in Table 4. This curve is an $E(B-V)$ weighted average of the five individual curves illustrated in Figures 3 and 4.

The extinction bump in the Orion extinction curve is weaker than in the average galactic curve. Using a straight line "background extinction" intersecting the curve at $\lambda^{-1} = 3.3$ μm^{-1} and 6.5 μm^{-1}, the maximum height of the bump above the straight line, $E(\text{bump})/E(B-V)$, is ~ 2.0 in the average Orion curve compared to 3.1 in the average galactic curve. While this bump strength as normalized by $E(B-V)$ is weaker toward the Orion stars, it peaks in strength at the normal wavelength, $\lambda_{max} \approx 2175$ Å. Foreground galactic extinction does not influence the conclusions reached with respect to dust in Orion, since Trapezium extinction derived using as star pairs θ^1 Ori D versus θ^1 Ori A and θ^2 Ori B, and θ^1 Ori C versus θ^2 Ori A (see Table 3) produced normalized extinction curves nearly identical to those illustrated in Figure 3.

The far-UV extinction in Orion is significantly smaller than in the average galactic curve. For example at $\lambda^{-1} = 8$ μm^{-1}, $\langle E(\lambda - V)/E(B-V)\rangle \approx 1.9$ compared to a galactic average of 6.5. If differences this large are typical in disturbed regions, then very large errors would be introduced if the standard extinction curve were used to correct for the effects of extinction toward such regions.

b) *HD 147889*

HD 147889 is a heavily reddened member of the ρ Oph reflection nebula. The *OAO 2* measurements of Bless and Savage (1972) for ρ Oph AB and σ Sco established the existence of peculiar UV extinction in this region. More recently Wu, Gilra, and van Duinen (1980) have presented *ANS* five-band photometry for HD 147889 and other stars in the ρ Oph cloud.

In Figure 4, the *IUE* results for HD 147889 are illustrated along with the average galactic curve and the curve for σ Sco from Bless and Savage (1972). The σ Sco curve is very similar to *OAO 2* measurements for ρ Oph AB. The visual and infrared extinction measurements for HD 147889 plotted in Figure 4 are from van Breda, Glass, and Whittet (1974) and McMillan (1978). For $\lambda^{-1} < 1.0$ these measurements deviate significantly from the average galactic curve and suggest a value of $R = A_V/E(B-V) \approx 4.1$. These data, combined with a larger than normal value for the wavelength of maximum visual polarization $\lambda_{max} = 0.80$ μm (Serkowski, Mathewson, and Ford 1975), imply that larger than normal grains are contributing to the visual and infrared extinction toward HD 147889.

The *IUE* extinction curve for HD 147889 is a striking counterexample to the curves obtained for the Orion Nebula stars. Toward HD 147889 the near-UV extinction bump is strong and peaks in strength at the normal wavelength, $\lambda_{max} \approx 2175$ Å. The bump has a normalized strength $E(\text{bump})/E(B-V) \approx 3.9$ when measured with respect to the straight line "background extinction" connecting the curve at $\lambda^{-1} = 3.3$ and 6.5 μm^{-1}. In contrast, the normal galactic curve has $E(\text{bump})/E(B-V) \approx 3.1$, while Orion has the value ≈ 2.0.

At far-UV wavelengths, the curve for HD 147889 first follows that for σ Sco and then abruptly turns upward for $\lambda^{-1} \gtrsim 7.0$ μm^{-1}. For $\lambda^{-1} \approx 8$ μm^{-1}, the curve for HD 147889 nearly joins up with the normal galactic curve. This very sudden increase in extinction toward HD 147889 has not been previously observed in extinction curves. The difference between the curves for σ Sco and HD 147889 implies the existence of an additional small particle component toward HD 147889.

IV. DISCUSSION

This investigation illustrates the great range over which the UV interstellar extinction curve can differ from place to place in the Galaxy. All the derived curves differ considerably from the average galactic curve of Savage and Mathis (1979). In one case (the Orion stars) the 2175 Å bump is relatively small, while in the other case (HD 147889) the normalized height of the bump is unusually large. At far-UV wavelengths, the Orion stars have a low and relatively flat extinction curve, while HD 147889 exhibits a curve that first follows that for σ Sco and then abruptly joins with the galactic average curve.

Detailed model fitting, which is beyond the scope of this investigation, will be required to explore the full implications of these new data. Even though the UV extinction curves illustrated in Figures 3 and 4 exhibit differences among themselves, the UV bump occurs at its normal position, $\lambda_{max} \approx 2175$ Å in all cases. In the case of the Orion stars and HD 147889, there is evidence that the grains responsible for the visual and infrared extinction are of a larger than normal size. If the grain species responsible for the UV bump were to also grow in size by mantle growth or coagulation, or become otherwise modified, one might expect the bump position to change (see Savage 1975; Mathis and Wallenhorst 1981), which is apparently not the case. In particular, if the bump is caused by small graphite grains, there must be some of

these grains in the Orion Nebula, even though the grains responsible for the visual extinction have a larger than normal size.

The strength of the bump in the various curves is of interest from the standpoint of grain destruction theories. Barlow (1978) has suggested that the implied deficiency of graphite grains in H II regions is due to "chemical sputtering" of graphite by H, N, and O atoms and ions. However, Draine (1979) has criticized Barlow' results and concludes that chemical sputtering is negligible in H II regions, although it could be important in regions where $n(\mathrm{H\ I}) > 10^5$ atoms cm^{-3} for 10^6 years or more. To account for the lower than normal strength of the 2175 Å feature toward Orion, Draine suggests a number of other possible destruction mechanisms.

The abrupt rise in the curve of HD 147889 for $\lambda^{-1} \gtrsim 7.0\ \mu\mathrm{m}^{-1}$ is surprising. This result demonstrates that, even in localized regions, extinction curves can be very different. (Compare the curves for σ Sco and HD 147889 in Fig. 4). Perhaps this upturn represents a new particle component. Even a molecular origin cannot be ruled out; the upturn has some resemblance to the absorption produced by H_2^+ (Stecher and Williams 1969; Heap and Stecher 1980).

In view of the wide range of curves found in this investigation, a word of caution is in order. Astronomers using an average galactic extinction curve to correct their data for the presence of UV extinction can make enormous errors. The normalized strength of the UV extinction bump does vary from region to region in the Galaxy. The common practice of using the mean galactic extinction curve to deredden observed flux distributions can lead to major errors. For an additional discussion of this problem see Meyer and Savage (1981).

We express our appreciation to the *IUE* staff at Goddard Space Flight Center for their assistance in acquiring and processing of the *IUE* data that appear in this paper. Dr. F. Fallon provided the precise astrometric coordinates for the Orion stars in advance of publication in Fallon (1981) that made the offset pointing possible for the Trapezium stars. Dr. C. Harvel, J. Heckathorn, and B. Coulter were very helpful in getting the early data reprocessed with the standard ITF files. W. Feibelman provided references and useful discussions on the variable stars in Orion. B. D. S. acknowledges support from NASA grants NSG 5241 and 5363.

REFERENCES

Anderson, C. M. 1970, *Ap. J.*, **160**, 507.
Baade, W., and Minkowski, R. 1937, **86**, 119.
Barlow, M. J. 1978, *M.N.R.A.S.*, **183**, 397.
Blanco, V. M., Demers, S., Douglass, G. G., and FitzGerald, M. P. 1970, *Pub. US Naval Obs.*, Vol. **13**.
Bless, R. C., and Savage, B. D. 1972, *Ap. J.*, **189**, 253.
Boggess, A., *et al.* 1978*a*, *Nature*, **275**, 372.
———. 1978*b*, *Nature*, **275**, 377.
Bohlin, R. C., and Holm, A. V. 1980, *IUE NASA Newsletter*, No. 10, p. 37.
Bohlin, R. C., Holm, A. V., Savage, B. D., Snijders, M. A. J., and Sparks, W. M. 1980, *Ast. Ap.*, **85**, 1.
Cassatella, A., Holm, A., Ponz, D., and Schiffer, F. H. 1980, *IUE NASA Newsletter*, No. 8, p. 1.
Draine, B. T. 1979, *Ap. J.*, **230**, 106.
Fallon, F. W. 1981, *A.J.*, in press.
Feibelman, W. A., and Gull, T. R. 1978, *Pub. A.S.P.*, **90**, 762.
Hall, D. S., and Garrison, L. M. 1969, *Pub. A.S.P.*, **81**, 771.
Heap, S., and Stecher, T. P. 1980, in *The Universe at Ultraviolet Wavelengths: The First Two Years of IUE*, ed. R. D. Chapman (NASA CP 2171).
Hoffleit, D. 1964, *Catalogue of Bright Stars* (New Haven: Yale University Observatory).
Johnson, H. L. 1966, *Ann. Rev. Astr. Ap.*, **4**, 193.
———. 1968, in *Nebulae and Interstellar Matter*, ed. B. M. Middlehurst and L. H. Aller (Chicago: University of Chicago Press), chap. 5.
Johnson, H. L. 1977, *Rev. Mexicana Astr. Ap.*, **2**, 175.
Lee, T. A. 1968, *Ap. J.*, **152**, 913.
Lesh, J. R. 1968, *Ap. J. Suppl.*, **16**, 371.
———. 1972, *Astr. Ap. Suppl.*,**5**, 129.
Mathis, J. S., and Wallenhorst, S. G. 1981, *Ap. J.*, **244**, 483.
McMillan, R. S. 1978, *Ap. J.*, **255**, 417.
Meyer, D. M., and Savage, B. D. 1981, *Ap. J.*, submitted.
Ney, E. P., Strecker, D. W., and Gehrz, R. D. 1973, *Ap. J.*, **180**, 807.
Panek, R. J., and Savage, B. D. 1976, *Ap. J.*, **206**, 167.
Patriarchi, P., and Perinotto, M. 1980, in *Proceedings of Second European IUE Conference* (Paris: European Space Agency, ESA-Sp 157), p. 201.
Savage, B. D. 1975, *Ap. J.*, **199**, 92.
Savage, B. D. and Mathis, J. S. 1979, *Ann. Rev. Astr. Ap.*, **17**, 73.
Schiffer, F. H. 1980, *IUE NASA Newsletter*, No. 11, p. 33.
Serkowski, K., Mathewson, D. S., and Ford, V. L. 1975, *Ap. J.*, **196**, 261.
Stebbins, J., and Whitford, A. E. 1945, *Ap. J.*, **102**, 318.
Stecher, T. P., and Williams, D. A. 1969, *Ap. Letters*, **4**, 99.
Strongylis, G. J., and Bohlin, R. C. 1979, *Publ. A.S.P.*, **91**, 205.
van Breda, I. G., Glass, I. S., and Whittet, D. C. B. 1974, *M.N.R.A.S.* **168**, 551.
Wilson, R. E. 1972, *Ap. Space Sci.*, **19**, 165.
Wu, C.-C., Gilra, D. P., and Van Duinen, R. J. 1980, *Ap. J.*, **241**, 173.

R. C. BOHLIN: NASA Goddard Space Flight Center, Code 681, Greenbelt, MD 20771

B. D. SAVAGE: Department of Astronomy, University of Wisconsin, 475 N. Charter St., Madison, WI 53706